Exploring the Impact of the Presence of 9,9'-Spirobifluorene Moieties on the Performance of Carbonyl-based Multiresonant Thermally Activated Delayed Fluorescence Organic Light-Emitting Diodes

Janine Haug, Sen Wu, Hassan Hafeez, Maximilian Schustek, Mahni Fatahi, Yannik T. Woordes, Martin Nieger, Olaf Fuhr, Burkhard Luy, Ifor D.W. Samuel*, Stefan Bräse*, Eli Zysman-Colman*

Janine Haug, Stefan Bräse
Institute of Biological and Chemical Systems - Functional Molecular Systems, Karlsruhe Institute of Technology (KIT), Kaiserstrasse 12, 76131 Karlsruhe, Germany. E-mail: braese@kit.edu

Janine Haug, Maximilian Schustek, Stefan Bräse
Institute of Organic Chemistry, Karlsruhe Institute of Technology (KIT), Kaiserstrasse 12, 76131 Karlsruhe, Germany. E-mail: braese@kit.edu

Janine Haug, Sen Wu, Mahni Fatahi, Eli Zysman-Colman
Organic Semiconductor Centre, EaStCHEM School of Chemistry, University of St Andrews, St Andrews KY16 9ST, Fife, UK. E-mail: eli.zysman-colman@st-andrews.ac.uk

Hassan Hafeez, Ifor D.W. Samuel
Organic Semiconductor Centre, SUPA School of Physics and Astronomy, University of St Andrews, St Andrews, Fife, KY16 9SS, UK. E-mail: idws@st-andrews.ac.uk

Yannik T. Woordes, Burkhard Luy
Institute for Biological Interfaces 4 – Magnetic Resonance, Karlsruhe Institute of Technology (KIT), Kaiserstrasse 12, 76131 Karlsruhe, Germany. E-mail: burkhard.luy@kit.edu

Martin Nieger
Department of Chemistry, University of Helsinki, P. O. Box 55 (A. I. Virtasen aukio 1), 00014 University of Helsinki, Finland. E-mail: martin.nieger@helsinki.fi

Olaf Fuhr
Institute of Nanotechnology (INT) and Karlsruhe Nano-Micro Facility (KNMFi), Karlsruhe Institute of Technology (KIT), Kaiserstrasse 12, 76131 Karlsruhe, Germany; E-mail: olaf.fuhr@kit.edu

Keywords: Thermally activated delayed fluorescence; organic light-emitting diodes; multiresonant thermally activated delayed fluorescence; spirobifluorene; structure-property relationship.

Abstract

The impact of the decoration of the multiresonant thermally activated delayed fluorescence (MR-TADF) core **DiKTa** with 9,9'-spirobifluorene (SBF) groups was investigated with respect to the impact of number, position, and incorporation-type of the SBF unit on the photophysical and optoelectronic properties. This approach allows for the development of narrowband, high-efficiency organic light emitting diodes (OLEDs) with moderate efficiency roll-off by alleviating aggregation-caused quenching. The MR-TADF emitters **DiKTaSBF**, **3-SBF-DiKTa**, **7-SBF-DiKTa**, and **7-SBF-DiKTaSBF**, differ in the number, position, and incorporation-type of the SBF unit. Sky-blue OLEDs with **DiKTaSBF** and **3-SBF-DiKTa** showed superior performance with maximal external quantum efficiencies (EQE_{max}) of 26.1 and 27.0%, respectively, while all four families of OLEDs showed a moderate efficiency roll-off. Narrowband emissions with full-width at half maximum (FWHM) of 32 and 35 nm were observed for 7-modified emitters, whereas for the devices with emitters containing SBF groups at the 3-position showed a broadened emission, with FWHM of about 50 nm. These findings highlight the effect of the regiochemistry of the SBF group on the optoelectronic properties and the corresponding impact on the performance of the OLEDs.

Introduction

Multiresonant thermally activated delayed fluorescence (MR-TADF) compounds introduced by Hatakeyama *et al*.,[1] have emerged as a promising class of emitters for use in organic light-emitting diodes (OLEDs). This is because unlike donor-acceptor TADF emitters, MR-TADF compounds show bright and narrowband emission, and therefore, the OLEDs emit with high color purity and high external quantum efficiency (EQE). MR-TADF emitters are typically fused p- and n-doped polyaromatic hydrocarbon compounds in which electron-rich donor and/or electron-deficient atoms are typically disposed *meta* to each other. This regiochemistry induces an alternating increasing and decreasing electron density distribution on adjacent atoms in the excited state, a pattern that is inverted compared to that in the ground state. This produces low-lying excited states of short-range charge transfer (SRCT) character, leading to suitably small singlet-triplet excited-state energy gaps (ΔE_{ST}) to enable TADF.[2]

The largest family of MR-TADF emitters contains boron atoms as the electron-accepting centers and oxygen and/or nitrogen atoms as donors. In 2019, Yuan *et al.* reported the first boron-free MR-TADF compound (**QAO**, aka **DiKTa**), substituting it for carbonyl moieties (Figure **1**).[3] The OLEDs with this emitter featured a narrowband sky-blue emission (λ_{EL} = 468 nm) and showed a maximum EQE (EQE_{max}) of 19.4%. By decorating this core structure of bulky mesityl substituents in the design of **Mes$_3$DiKTa** (Figure **1**), we demonstrated that the aggregation-caused quenching (ACQ) inherent in the parent could be mitigated, evidenced by a higher EQE_{max} of 21.2%.[4]

Substituent regiochemistry can have an impact on the photophysics of the emitter. For instance, Li *et al.* investigated the effect of the regiochemistry of a phenyl substituent on the DiKTa core on the photophysical properties of the emitter, contrasting the properties of **3-PhQAD** and **7-PhQAD** (Figure **1**).[5] In 2 wt% doped films in mCP, both compounds show similar photophysical properties, though the emission of **3-PhQAD** is slightly red-shifted at λ_{PL} of 478 nm and there is a small increase in the photoluminescence quantum yield, Φ_{PL}, to 73% compared to **7-PhQAD**, which emits at 472 nm and has a Φ_{PL} of 68%. The device EQE_{max} are comparable across the OLEDs with **DiKTa**, **3-PhQAD**, and **7-PhQAD** as emitters, showing EQE_{max} of 19.4, 19.1, and 18.8%, respectively. The trend in the PL is mirrored in the electroluminescence (EL) spectra where the devices with **3-PhQAD** have the most red-shifted and broadened EL (λ_{EL} of 480 nm, FWHM of 44 nm [233 meV]) compared to those with **7-PhQAD** (λ_{EL} of 472 nm, FWHM of 34 nm [184 meV]) and **DiKTa**[3] (λ_{EL} of 468 nm, FWHM of 39 nm [225 meV]).

(a)

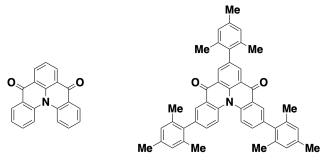

DiKTa
λ_{PL} = 465 nm
FWHM = 37 nm
ΔE_{ST} = 0.20 eV
Φ_{PL} = 75%
EQE_{max} = 14.7%
(3.5 wt% doped in mCP)

Mes_3DiKTa
λ_{PL} = 477 nm
FWHM = 37 nm
ΔE_{ST} = 0.21 eV
Φ_{PL} = 80%
EQE_{max} = 21.1%
(3.5 wt% doped in mCP)

Adv. Opt. Mater. **2019**, *7*, 1801536
Adv. Opt. Mater. **2020**, *8*, 1901627

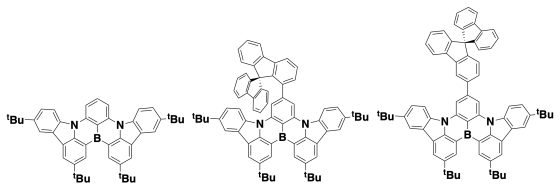

BNCz
λ_{PL} = 485 nm
FWHM = 27.5 nm
ΔE_{ST} = 0.14 eV
(toluene)
Φ_{PL} = 81%
EQE_{max} = 23.9%
(2 wt% doped in mCBP)

SF1BN
λ_{PL} = 493 nm
FWHM = 27.5 nm
ΔE_{ST} = 0.13 eV
(toluene)
Φ_{PL} = 93%
EQE_{max} = 35.9%
(2 wt% doped in mCBP)

SF3BN
λ_{PL} = 493 nm
FWHM = 28.0 nm
ΔE_{ST} = 0.15 eV
(toluene)
Φ_{PL} = 90%
EQE_{max} = 31.7%
(2 wt% doped in mCBP)

Angew. Chem. Int. Ed. **2022**, *61*, e202201886

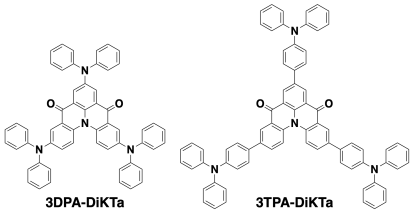

3DPA-DiKTa
λ_{PL} = 617 nm
FWHM = 56 nm
ΔE_{ST} = 0.20 eV
Φ_{PL} = 60%
EQE_{max} = 16.7%
(2 wt% doped in mCP)

3TPA-DiKTa
λ_{PL} = 551 nm
FWHM = 58 nm
ΔE_{ST} = 0.13 eV
Φ_{PL} = 93%
EQE_{max} = 30.8%
(2 wt% doped in mCP)

Angew. Chem. Int. Ed. **2022**, *61*, e202213697

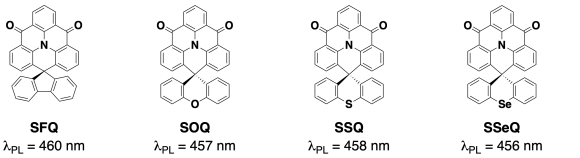

SFQ
λ_{PL} = 460 nm
FWHM = 30 nm
ΔE_{ST} = 0.20
Φ_{PL} = 98.3%
EQE_{max} = 21.7%
(3 wt% doped in mCBP)

SOQ
λ_{PL} = 457 nm
FWHM = 32 nm
ΔE_{ST} = 0.21
Φ_{PL} = 95.2%
EQE_{max} = 24.3%
(3 wt% doped in mCBP)

SSQ
λ_{PL} = 458 nm
FWHM = 30nm
ΔE_{ST} = 0.21
Φ_{PL} = 92.0%
EQE_{max} = 25.5%
(3 wt% doped in mCBP)

SSeQ
λ_{PL} = 456 nm
FWHM = 34 nm
ΔE_{ST} = 0.22
Φ_{PL} = 96.2%
EQE_{max} = 22.2%
(3 wt% doped in mCBP)

Angew. Chem. Int. Ed. **2023**, *62*, e202310047

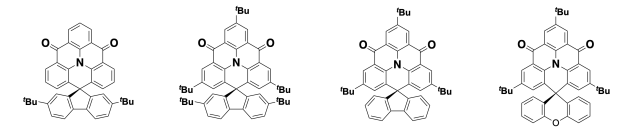

QAO-TF
λ_{PL} = 461 nm
FWHM = 42 nm
ΔE_{ST} = 0.22 eV (toluene)
Φ_{PL} = 98%
(2 wt% doped in mCBP)
EQE_{max} = 23.3%
(4 wt% doped in mCBP)

TQAO-TF
λ_{PL} = 472 nm
FWHM = 23 nm
ΔE_{ST} = 0.20 eV (toluene)
Φ_{PL} = 97%
(2 wt% doped in mCBP)
EQE_{max} = 30.9%
(4 wt% doped in mCBP)

TQAO-F
λ_{PL} = 473 nm
FWHM = 23 nm
ΔE_{ST} = 0.20 eV (toluene)
Φ_{PL} = 97%
(2 wt% doped in mCBP)
EQE_{max} = 31.7%
(4 wt% doped in mCBP)

TSOQ
λ_{PL} = 469 nm
FWHM = 22 nm
ΔE_{ST} = 0.24 eV (toluene)
Φ_{PL} = 98%
(2 wt% doped in mCBP)
EQE_{max} = 30.0%
(4 wt% doped in mCBP)

Small **2025**, 2502915

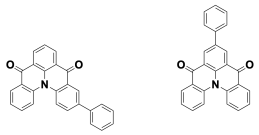

3-PhQAD
λ_{PL} = 478 nm
FWHM = 30 nm (toluene)
ΔE_{ST} = 0.18 eV
Φ_{PL} = 73%
EQE_{max} = 19.1%
(2 wt% doped in mCP)

7-PhQAD
λ_{PL} = 472 nm
FWHM =22 nm (toluene)
ΔE_{ST} = 0.19 eV
Φ_{PL} = 68%
EQE_{max} = 18.7%
(2 wt% doped in mCP)

Appl. Mater. Interfaces **2019**, *11*, 13472

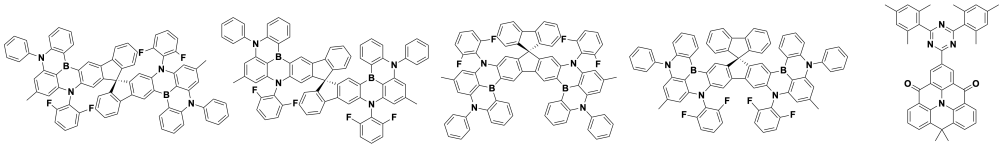

SF-BN1
λ_{PL} = 458 nm
FWHM = 17 nm
ΔE_{ST} = 0.09 eV
(toluene)
Φ_{PL} = 93.1% (1 wt%)
EQE_{max} = 26.3% (3 wt%)
(doped in p-PhBCzPh)

SF-BN2
λ_{PL} = 463 nm
FWHM = 21 nm
ΔE_{ST} = 0.09 eV
(toluene)
Φ_{PL} = 90.3% (1 wt%)
EQE_{max} = 22.0% (2 wt%)
(doped in p-PhBCzPh)

SF-BN3
λ_{PL} = 471 nm
FWHM = 17 nm
ΔE_{ST} = 0.06 eV
(toluene)
Φ_{PL} = 97.2% (1 wt%)
EQE_{max} = 29.8% (2 wt%)
(doped in p-PhBCzPh)

SF-BN4
λ_{PL} = 483 nm
FWHM = 15 nm
ΔE_{ST} = 0.07 eV
(toluene)
Φ_{PL} = 96.5% (1 wt%)
EQE_{max} = 32.2% (3 wt%)
(doped in p-PhBCzPh)

MTMDQAO
λ_{PL} = 470 nm
FWHM =37 nm
ΔE_{ST} = 0.20 eV (in solution)
Φ_{PL} = 99%
EQE_{max} = 29.4%
(10 wt% doped in mCP)

Angew. Chem. Int. Ed. **2025**, e202504723

Sci. China Chem. **2024**, *67*, 351

(b) *This work*

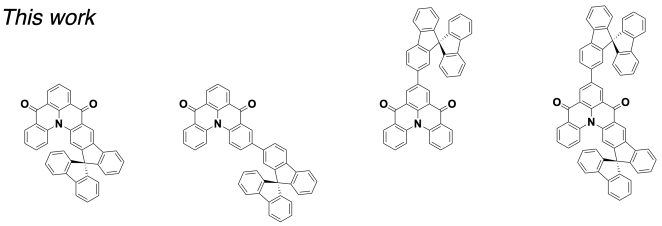

DiKTaSBF
λ_{PL} = 490 nm
FWHM = 41 nm
ΔE_{ST} = 0.18 eV
Φ_{PL} = 82%
EQE_{max} = 26.1%
(2 wt% doped in 26DCzPPy)

3-SBF-DiKTa
λ_{PL} = 489 nm
FWHM = 49 nm
ΔE_{ST} = 0.26 eV
Φ_{PL} = 72%
EQE_{max} = 27.0%
(2 wt% doped in 26DCzPPy)

7-SBF-DiKTa
λ_{PL} = 484 nm
FWHM = 32 nm
ΔE_{ST} = 0.20 eV
Φ_{PL} = 71%
EQE_{max} = 20.5%
(2 wt% doped in 26DCzPPy)

7-SBF-DiKTaSBF
λ_{PL} = 496 nm
FWHM = 35 nm
ΔE_{ST} = 0.25 eV
Φ_{PL} = 75%
EQE_{max} = 20.1%
(2 wt% doped in 26DCzPPy)

Figure **1**. (a) Literature survey of spiro-modified MR-TADF emitters. (b) Structures and properties of emitters introduced in this study.

Exploring the potential of DiKTa-based emitters, we later showed that the emission could be tuned towards the red and that the orientation of the transition dipole moment (TDM) of the emitter could be induced to be strongly horizontally aligned with the substrate as a function of the number and strength of peripheral electron-donating substituents, exemplified in green and red narrowband-emitting devices with **3TPA-DiKTa** and **3DPA-DiKTa** (Figure **1**), respectively, showing EQE_{max} of 30.8 and 17.9%.[6] Despite this performance, it is actually reasonably challenging to *a priori* design emitters whose TDM is preferentially horizontally oriented.[7] Empirically, one promising approach for enhancing the horizontal orientation of the TDM is to incorporate 9,9'-spirobifluorene (SBF) groups.[7]

Following this approach, there have been several reports of MR-TADF emitters incorporating spiro-units. Qu *et al.* reported two regioisomeric emitters **SF1BN** and **SF3BN** based on the **BNCz** (Figure **1**) containing a SBF unit attached either at C1 or C3, respectively.[8] A significant increase in the device EQE_{max} was observed from 23.9% with **BNCz** to 35.9 and 32.2% for the devices with **SF1BN** and **SF3BN**, respectively. These outstanding device efficiencies were attributed to the high horizontal orientation of the TDMs of 95 and 96% for **SF1BN** and **SF3BN**, respectively.

Yu *et al*. published a series of four emitters **SFQ**, **SOQ**, **SSQ**, and **SSeQ** (Figure **1**) introducing spiro-locks into the DiKTa core.[9] The emitter **SFQ** has a near unity photoluminescence quantum yield, Φ_{PL}, of 98.3% (3 wt% doped in mCBP), which is higher compared to the 75% reported for **DiKTa** (3.5 wt% doped in mCP). Further, the enhanced rigidity resulted in a narrowed emission reflected in the full-width at half maximum, FWHM, of 30 nm [172 meV] (3 wt% doped in mCBP; **DiKTa**: 37 nm [204 meV], 3.5 wt% doped in mCP). The incorporation of the spiro center resulted in an improved EQE_{max} of 21.7% compared to the 14.7% for the device with **DiKTa**, attributed by the authors to reduced quenching. Exploring the effect of the decoration of **SFQ** and **SOQ** with *tert*-butyl groups, Yan *et al.* reported a series of four emitters (**QAO-TF**, **TQAO-TF**, **TQAO-F**, and **TSOQ**, Figure **1**). Modification of the DiKTa core structure with three *tert*-butyl groups resulted in a significant increase in the device EQE_{max} of 30.9, 31.7, and 30.0% for the devices with **TQAO-TF**, **TQAO-F**, and **TSOQ,** compared to 21.7% and 24.3% for the devices with **SFQ** and **SOQ**, respectively.[10] In contrast, there was only a moderate increase in the EQE_{max} of the device with **QAO-TF** (EQE_{max} of 23.3%) compared to the device with **SFQ**, where *tert*-butyl substitution is only on the spirofluorene. In 2 wt% doped films in mCBP, all four emitters showed near-unity Φ_{PL} of 97 to 98%, similar to the 98.3 and 95.2% reported for **SFQ** and **SOQ**, respectively. Further, the 3 wt% doped films in mCBP of **TQAO-TF**, **TQAO-F**, and **TSOQ** showed narrowband emission, with FWHM of 23, 23, and 22 nm [127, 126, and 122 meV], respectively, which are narrower compared to 30 nm [172 meV] for **SFQ**, and 32 nm [185 meV] for **SOQ**. In contrast, **QAO-TF** showed broadened emission to 42 nm [235 meV]. Remarkably, the devices with **TQAO-TF**, **TQAO-F**, and **TSOQ** achieved to date some of the highest EQE_{max} among unsensitized blue OLEDs of DiKTa-based emitters (Figure **2**).

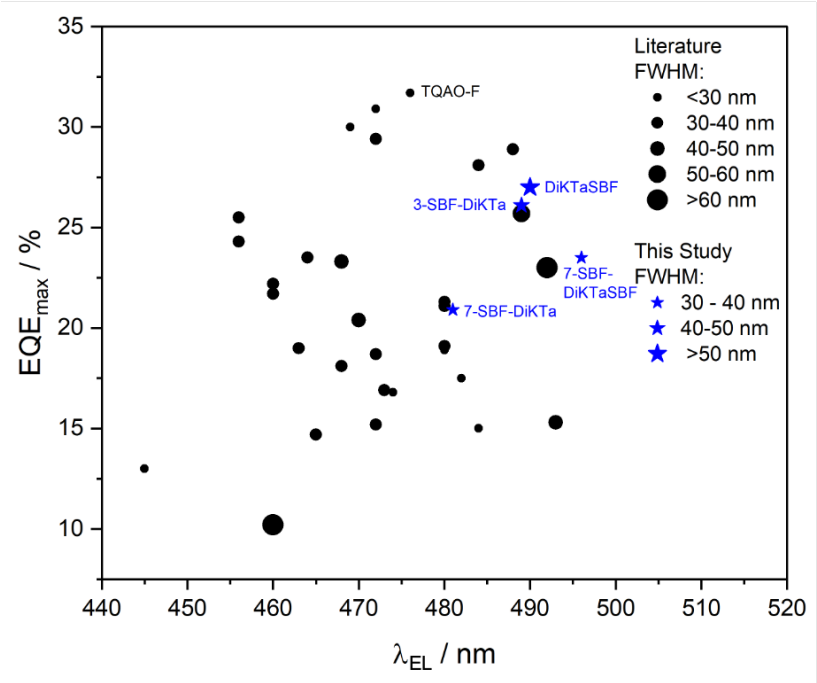

Figure **2**. Literature survey of unsensitized blue OLEDs with DiKTa-based emitters (black circles) and the emitters reported in this study (blue stars). The size of the data point is proportional to the EL FWHM of the emitter.

In 2025, Wu *et al.* reported four emitters, **SF-BN1**, **SF-BN2**, **SF-BN3**, and **SF-BN4**, consisting of two **DABNA-1**-type moieties that are fused on different fluorene fragments of the SBF.[11] **SF-BN1** and **SF-BN2** emit in the deep-blue in toluene with λ_{PL} of 458 and 463 nm, respectively, while **SF-BN3** and **SF-BN4** emit at λ_{PL} of 471 and 483 nm, respectively. All four compounds show very narrowband emission, with FWHM ranging from 15 to 21 nm [79.3 to 99.9 meV]. In 1 wt% doped films in p-PhBCzPh, the Φ_{PL} values exceeded 90%, with the highest value of 97.2% for **SF-BN3**. The resulting EQE_{max} increased from 22.0% for the device with device **SF-BN2** to 26.3% for the device with **SF-BN1**, reaching 29.8 and 32.2% for devices with **SF-BN3** and **SF-BN4**, respectively. These results highlight the great potential of the SBF fusion strategy.

Here, we report four narrowband sky-blue SBF-decorated **DiKTa** derivatives; **DiKTaSBF**, **3-SBF-DiKTa**, **7-SBF-DiKTa** and **7-SBF-DiKTaSBF** (Figure **1**). These emitters differ in the number, regiochemistry, and point of attachment of the SBF unit. From this study, structure-property relationships become apparent, with decoration at the 7-position of **DiKTa** favoring a narrowband emission, while substitution at the 3-position resulted in both higher EQE_{max} and reduced efficiency roll-off, resulting in device EQE_{max} of up to 27.0%. This value is among the highest EQE_{max} reported to date for unsensitized blue OLEDs with DiKTa-based emitters, highlighting the potential of spiro-decoration and carbonyl/nitrogen-based emitters.

Synthesis

The syntheses of **DiKTaSBF**, **7-SBF-DiKTa**, and **7-SBF-DiKTaSBF** are shown in Figure **3** and the synthesis of **3-SBF-DiKTa** is shown Figure **4**. In general, two synthetic routes were developed: one for accessing the SBF-fused and/or 7-position modified emitters **DiKTaSBF**, **7-SBF-DiKTa** and **7-SBF-DiKTaSBF**, which are elaborated from **7-Br-DiKTa**[12], and another based on the availability of intermediate **3-I-DiKTa**[13] to access **3-SBF-DiKTa**.

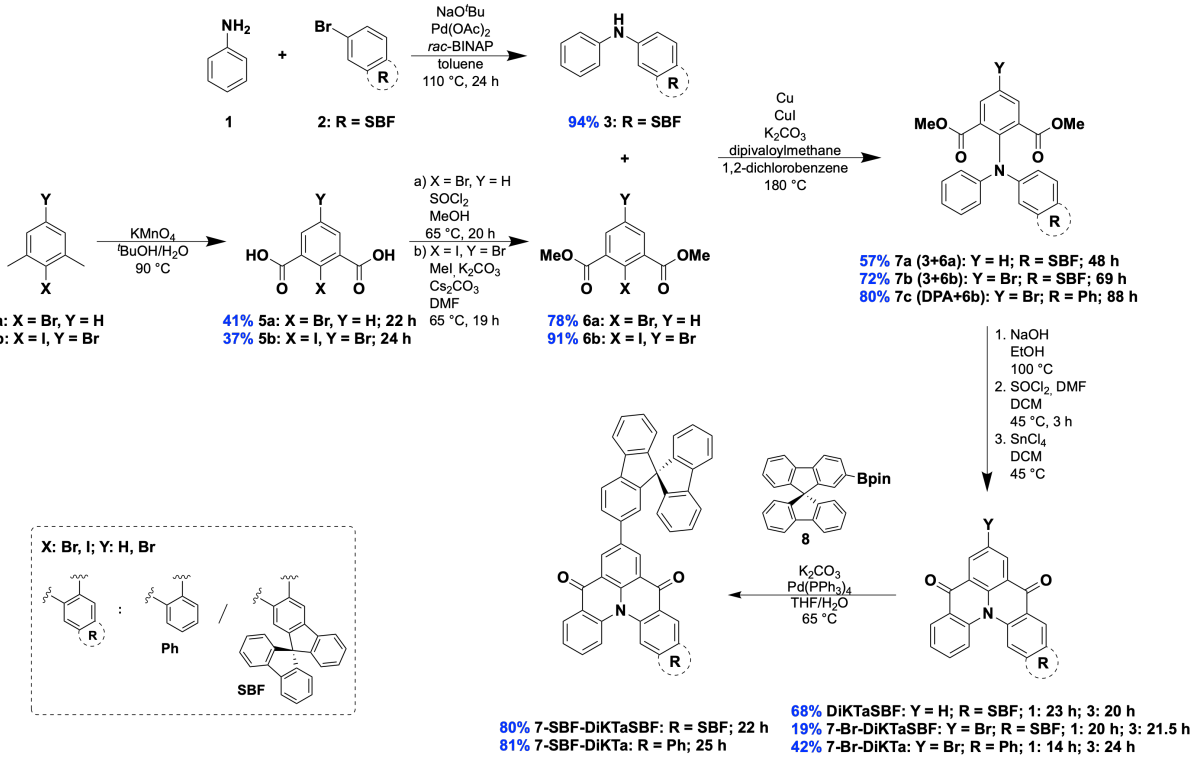

Figure **3**. Synthetic route accessing **DiKTaSBF**, **7-SBF-DiKTa**, and **7-SBF-DiKTaSBF**.

Following the established protocol towards **7-Br-DiKTa**,[12] the first step comprised the preparation of the halogenated dimethyl isophthalates (**6a, 6b**) in two steps *via* an oxidation and methylation sequence. Subsequently, these were coupled either with diphenylamine (**DPA**) or *N*-phenyl-9,9'-spirobi[fluoren]-2-amine (**3a**) using Ullmann conditions, affording **7a**-**7c** in fair-to-good yields of 57, 72, and 80%, respectively. The intermediate **3a** was prepared *via* a Buchwald-Hartwig amination in an excellent yield of 94%. Friedel-Craft-type ring closure reactions yielded the emitter **DiKTaSBF**, as well as the intermediates **7-Br-DiKTa** and **7-Br-DiKTaSBF**, in yields of 68, 42, and 19%, respectively. Optimization for the synthesis of **7-Br-DiKTaSBF** was attempted by varying the chlorinating agent between oxalyl chloride and thionyl chloride, as well as the Lewis acid between tin(IV) chloride and aluminum(III) chloride; however, neither strategy yielded any improvement. Incorporation of the SBF unit at the 7-position was realized via a Suzuki-Miyaura cross-coupling with (9,9'-spirobi[fluorene]-4-yl)boronic acid pinacol ester, yielding 81% of **7-SBF-DiKTa** and 80% of **7-SBF-DiKTaSBF**.

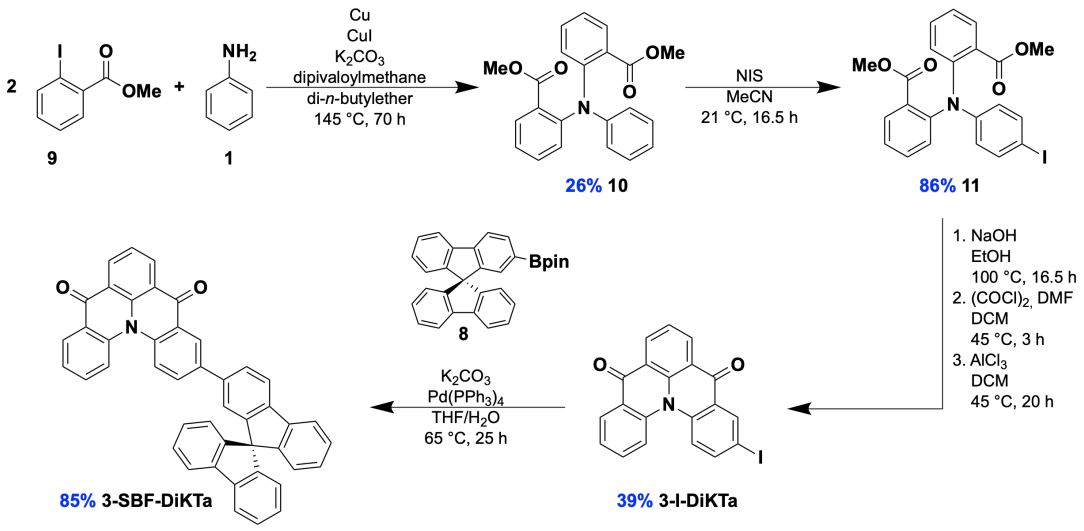

Figure **4**. Synthetic route for **3-SBF-DiKTa**.

For modification at the 3-position, **3-I-DiKTa** was prepared in an overall yield of 9% according to a literature procedure[13] in three steps consisting of a sequence of Ullmann-coupling, iodination and Friedel-Craft-type ring closure reactions. Subsequently, the emitter **3-SBF-DiKTa** was prepared via a Suzuki-Miyaura cross-coupling between **3-I-DiKTa** and (9,9'-spirobi[fluoren]-4-yl)boronic acid pinacol ester (**8**) in an 85% yield.

The emitters were characterized by a combination of ^{1}H, ^{13}C NMR and 2D NMR spectroscopy (Figures **S1-S34**), infrared spectroscopy (Figures **S52-68)**, high-resolution mass spectrometry (Figures **S35-S51**), elemental analysis (Figures **S69-S71**), and high-performance liquid chromatography (Figures **S72-S75**), confirming the structures and their purity.

Thermal Stability

The thermal stability was evaluated via thermogravimetric analysis (TGA) and differential scanning calorimetry (DSC) (Figure **S78a**). All compounds are thermally stable, with 5% mass loss (T_d) at 380, 358, 432, and 405 °C for **DiKTaSBF**, **3-SBF-DiKTa**, **7-SBF-DiKTa**, and **7-SBF-DiKTaSBF**, respectively. Consequently, all emitters possess an enhanced thermal stability compared to **DiKTa**, which has a reported T_d value of 323 °C.[4] No glass transitions were observed in the DSC traces (Figure **S78b**).

Structural Characterization

The molecular structures of **DiKTaSBF** (Figure **S76**) and **7-SBF-DiKTaSBF** (Figure **S77**) were confirmed by single crystal X-ray diffraction studies. Crystals were grown by slow evaporation of a mixture of petroleum ether and THF. In both cases, a centrosymmetric space group is present. As a result, the unit cells of both emitters comprise both atropisomers, differing in the relative orientation at the helical pitch. Both isomers of **DiKTaSBF** and **7-SBF-DiKTaSBF** are shown in Figure **S79**.

Significant line-broadening was observed in the ^{1}H and ^{13}C NMR spectra of all three SBF-fused compounds (**DiKTaSBF**, **7-Br-DiKTaSBF** and **7-SBF-DiKTaSBF**) when recorded at room temperature. Well-resolved spectra were recorded at 0 °C, allowing the assignment of the broadened resonances to the orthogonal fluorene unit of the fused SBF (Figures **S85-89**). This phenomenon is attributed to the conformational flexibility of the atropisomers. Temperature-dependent ^{1}H and ^{13}C NMR spectroscopy measurements (Figures **S90-S91**) evidence the fluctional behavior of the emitters with increasing temperature, with the resonances at 6.6, 7.0-7.1, 7.9 and 8.3 ppm coalescing at about 318 K. The barrier to isomerization was too high to be measured by variable temperature NMR spectroscopy.

Quantum Chemical Calculations

The frontier molecular orbitals (FMOs) were modelled using density function theory (DFT) at the PBE0/6-31G(d,p) level of theory in toluene.[14] The electron density plots of the highest occupied molecular orbital (HOMO) and lowest unoccupied molecular orbital (LUMO) are shown in Figure **5a** and the values are summarized in Table **1**. The calculated HOMO energies range between -5.95 and -5.78 eV. **DiKTaSBF** has the most stabilized HOMO at -5.95 eV, followed by **3-SBF-DiKTa** and **7-SBF-DiKTa** that have nearly isoenergetic HOMOs at respectively -5.86 and -5.84 eV, while the most destabilized HOMO of -5.78 eV is for **7-SBF-DiKTaSBF**. Compared to **DiKTa** (-6.21 eV), the HOMO is destabilized in each of these emitters, likely due the extended conjugation into the SBF units. The HOMO density of **DiKTaSBF** only extends into the fused fluorene unit and not the orthogonal one, whereas in the coupled emitters **3-SBF-DiKTa** and **7-SBF-DiKTa**, the HOMO density extends into both fluorene units. Given the presence of two SBF units in **7-SBF-DiKTaSBF**, the most destabilized HOMO is in this compound. In contrast, nearly identical LUMO energies were computed for all the emitters, ranging narrowly from -2.25 to -2.28 eV, these are similar to the LUMO of **DiKTa** (-2.29 eV). This indicates a LUMO that is localized about the central DiKTa core as is also evident from the plots in Figure **5a**. Consequently, the computed HOMO-LUMO gaps range between 3.53 and 3.70 eV, which are smaller than that of **DiKTa** (3.92 eV), indicating that the absorption and emission of the emitters are likely to be red-shifted compared to those of the parent, **DiKTa**.

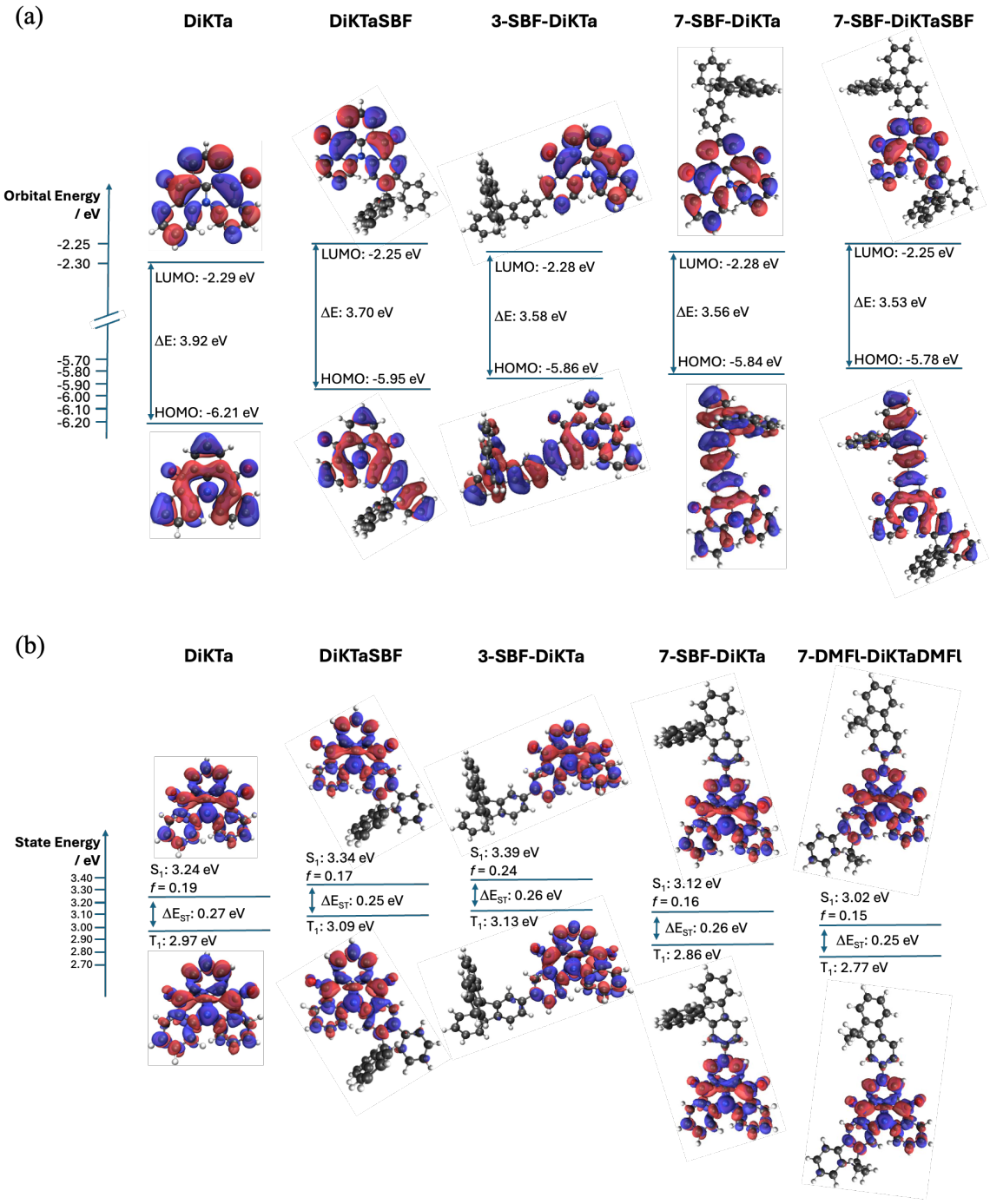

Figure **5**.(a) Calculated FMOs in toluene at the PBE0/6-31G(d,p) level of **DiKTa**, **DiKTaSBF**, **3-SBF-DiKTa**, **7-SBF-DiKTa**, and **7-SBF-DiKTaSBF** (isovalue of 0.02); (b) Difference density plots of S_1 and T_1 states with the corresponding energies calculated at the SDS-ADC(2)/cc-pVDZ level for **DiKTa**, **DiKTaSBF**, **3-SBF-DiKTa**, **7-SBF-DiKTa** and **7-DMFl-DiKTaDMFl** (isovalue of 0.001).

Given that TD-DFT calculations neglect higher-order excitations, the ΔE_{ST} of MR-TADF emitters commonly is overestimated at this level of theory.[14] Therefore, for a more accurate modelling, computations at the RI-SCS-ADC(2)/cc-pVDZ level of theory were performed (Figure **5b**), as double excitations are included at this level of theory. The calculated ΔE_{ST} values are essentially the same across this family of emitters, ranging between 0.25 and 0.26 eV. These are sufficiently small and of similar magnitude to 0.27 eV for **DiKTa** (SCS-CC2/cc-pVDZ),[4] 0.26 eV for **Mes$_3$DiKTa** (SCS-CC2/cc-

pVDZ),[4] and 0.27 eV for **PCP-DiKTa** (SCS-CC2/cc-pVDZ)[15] that reverse intersystem crossing (RISC) is expected to be operational to promote TADF. Due to the increased computational demand of the larger analog **7-SBF-DiKTaSBF**, we modelled a simplified structure **7-DMFl-DiKTaDMFl** (Figure **S80**), wherein the orthogonal fluorene units were replaced with geminal dimethyl groups. The energies of the first excited singlet state, S_1, of the 3-modified emitters **DiKTaSBF** (3.34 eV) and **3-SBF-DiKTa** (3.39 eV) are computed to be higher than that of **DiKTa** (3.24 eV). In contrast, the S_1 states of **7-SBF-DiKTa** (3.12 eV) and **7-DMFl-DiKTaDMFl** (3.02 eV) are more stabilized. An identical trend was observed for the T_1 energies, which are higher for **DiKTaSBF** (3.09 eV) and **3-SBF-DiKTa** (3.13 eV) and lower for **7-SBF-DiKTa** (2.86 eV) and **7-DMFl-DiKTaDMFl** (2.77 eV) compared to **DiKTa** (2.97 eV). The difference density plots reveal the expected alternating pattern of increasing and decreasing electron density characteristic of MR-TADF emitters, and there are no significant differences compared to the difference density plot of **DiKTa** (Figure **5b**). Similar to **DiKTa** (f = 0.19), the S_0-S_1 transition for each of these compounds has a predicted oscillator strength, f, ranging between 0.15 and 0.24.

Table **1**. Summary of calculated data.

	HOMO /eV [a]	**LUMO /eV** [a]	**ΔE /eV** [a]	**S_1 /eV** [b]	**T_1 /eV** [b]	**ΔE_{ST} /eV** [b]	**f** [b]
DiKTa	-6.21	-2.29	3.92	3.24	2.97	0.27	0.19
DiKTaSBF	-5.95	-2.25	3.70	3.34	3.09	0.25	0.17
3-SBF-DiKTa	-5.86	-2.28	3.58	3.39	3.13	0.26	0.24
7-SBF-DiKTa	-5.84	-2.28	3.56	3.12	2.86	0.26	0.16
7-SBF-DiKTaSBF	-5.78	-2.25	3.53	-	-	-	-
7-DMFl-DiKTaDMFl [c]	-5.77	-2.26	3.51	3.02	2.77	0.25	0.15

Calculated at the [a] PBE0/6-31G(d,p) level in toluene and [b] SCS-ADC(2)/cc-pVDZ level of theory in the gas phase. [c] Values based on a simplified model compound where the orthogonal fluorene units in **7-SBF-DiKTaSBF** have been replaced with *gem*-dimethyl groups.

Electrochemistry

Differential pulse voltammetry (DPV) and cyclic voltammetry (CV) spectra were recorded in degassed dichloromethane (DCM) solutions with tetrabutylammonium hexafluorophosphate as the supporting electrolyte. The voltammograms are shown in Figure **6**, and the data is summarized in Table **2**. The data were used to infer the HOMO and LUMO energies.

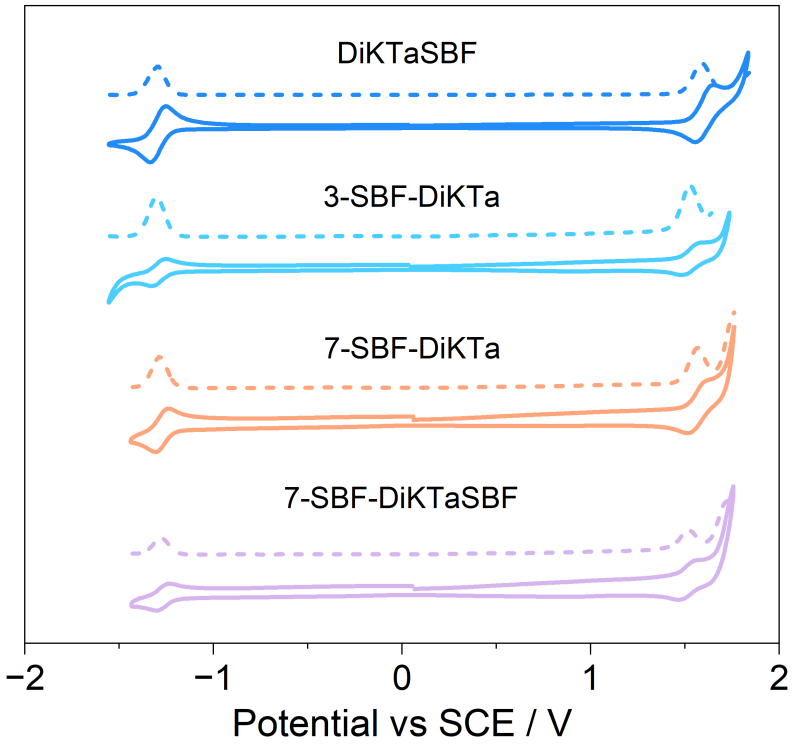

Figure **6**. CV and DPV curves of **DiKTaSBF**, **3-SBF-DiKTa**, **7-SBF-DiKTa**, and **7-SBF-DiKTa** in degassed DCM with 0.1 M [^{n}Bu$_4$N]PF$_6$ as the supporting electrolyte and Fc/Fc$^+$ as the internal reference. The voltammograms are referenced versus SCE (0.46 V vs. SCE).[16]

All emitters showed reversible oxidation and reduction waves. Similar oxidation, E_{ox}, and reduction, E_{red}, potentials were measured for all emitters, ranging between 1.52 and 1.59 eV for E_{ox}, and -1.28 and -1.30 eV for E_{red}. Compared to the redox potentials of **DiKTa** in DCM reported in the literature,[17] all emitters possess a less positive E_{ox} (**DiKTa**: 1.78 V) and a similar E_{red} (**DiKTa**: -1.35 V). The HOMO and LUMO energies in DCM range from -5.86 to -5.93 eV and -3.04 to -3.06 eV, respectively. Not surprisingly, no significant modulation of the LUMO (-3.02 eV for **DiKTa**) was observed. However, the HOMO levels of the four emitters are destabilized compared to **DiKTa** (-6.12 eV). These trends are in line with the computations. The resulting electrochemical gaps, ΔE_{redox}, are thus similar among the emitters, ranging from 2.80 and 2.89 V. This implies that the incorporation type, position, and number of the SBF unit(s) does not significantly impact the HOMO and LUMO levels, but its inclusion does lead to a destabilization of the HOMO compared to **DiKTa**, in line with the calculations. Compared to the ΔE_{redox} of 3.10 eV for **DiKTa**, all emitters thus have a smaller ΔE_{redox}.

Table **2**. Summary of the electrochemistry.

	E_{ox}[a] / v *vs.* SCE	E_{red}[a] / v *vs.* SCE	HOMO[b] / eV	LUMO[b] / eV	ΔE_{redox}[c] / eV
DiKTa[17]	1.78	-1.35	-6.12	-3.02	3.10
DiKTaSBF	1.59	-1.30	-5.93	-3.04	2.89
3-SBF-DiKTa	1.53	-1.30	-5.87	-3.04	2.83
7-SBF-DiKTa	1.57	-1.29	-5.91	-3.05	2.86
7-SBF-DiKTaSBF	1.52	-1.28	-5.86	-3.06	2.80

[a] Measured in DCM (0.46 V for DCM/ vs SCE)[16] at a scan rate of 0.1 V/s. [b] HOMO and LUMO energies were determined using $E_{HOMO/LUMO}$ = - (E_{ox}/E_{red}+4.8) eV where E_{ox} and E_{red} are onset of anodic and cathodic peak potentials, respectively, calculated from DPV versus Fc/Fc^{+}.[18] [c] $\Delta E_{redox} = |E_{HOMO}-E_{LUMO}|$.

Photophysical measurements

The photophysical properties of the four emitters are summarized in Table **3**. Their absorption and emission spectra (Figure **7**) in dilute toluene solutions (10^{-5} M) show the expected mirror image profile at room temperature and small Stokes shifts (21-28 nm) that indicate that there is only a small geometry relaxation in the excited state owing to their relatively rigid structures. The steady-state photoluminescence (SS PL) spectra reveal that these compounds emit sky-blue, with photoluminescence maxima, λ_{PL}, ranging from 470 nm for **7-SBF-DiKTa**, 474 and 475 nm for **3-SBF-DiKTa** and **DiKTaSBF**, to 485 nm for **7-SBF-DiKTaSBF**. All compounds show narrowband emission, with FWHM of 26, 29, 35, and 39 nm (144, 151, 183, and 202 meV) for **7-SBF-DiKTa**, **7-SBF-DiKTaSBF**, **3-SBF-DiKTa**, and **DiKTaSBF**, respectively. Compared to **DiKTa**,[17] which emits at λ_{PL} of 453, the emission of these derivatives is red-shifted, which is consistent with their narrower HOMO-LUMO gaps. The PL of the 7-substituted derivatives is not significantly broadened compared to **DiKTa**, whereas a broadening was observed for the 3-substituted derivatives. All of these compounds exhibit weak positive solvatochromism (Figure **S81**), indicating that the nature of the emissive excited state remains SRCT across these solvents.

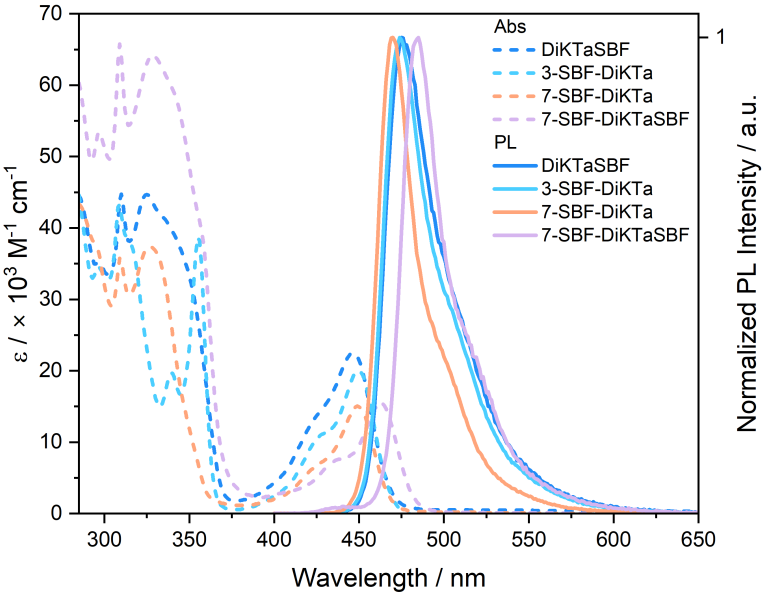

Figure **7**. Absorption and photoluminescence spectra of **DiKTaSBF**, **3-SBF-DiKTa**, **7-SBF-DiKTa**, and **7-SBF-DiKTaSBF** in dilute toluene (10^{-5} M, λ_{exc} = 340 nm).

The time-resolved PL decays in degassed toluene solution are shown in Figure **S82**. In toluene the PL decays with monoexponential kinetics for each of the prompt fluorescence lifetime, τ_p and delayed fluorescence lifetime, τ_d. All four emitters have similarly short τ_p ranging from 5.42 to 6.18 ns, which are in line with the τ_p of 5.1 ns reported for **DiKTa**.[17] In contrast, a more significant difference was observed for the delayed emission lifetimes τ_d, ranging between 71.5 and 107 µs. **7-SBF-DiKTa** features the shortest τ_d with 71.5 µs, followed by **DiKTaSBF** and **7-SBF-DiKTaSBF** with similar τ_d of 88.7 and 90.5 µs, respectively. The longest τ_d of 107 µs is present in **3-SBF-DiKTa**.

The ΔE_{ST} was determined from the onsets of the steady-state PL and phosphorescence spectra at 77 K in 2-MeTHF glass (Figure **S83**). The ΔE_{ST} values in 2-MeTHF range narrowly between 0.20 and 0.25 eV, which align with the computed values. These values are similar to other derivatives of **DiKTa**; for instance, ΔE_{ST} values of 0.23 eV for **SFQ** (in toluene),[9] 0.21 eV for **3DPA-DiKTa** (in 2-MeTHF),[6] and 0.16 eV for **PCP-DiKTa** (in 2-MeTHF) have been reported.[15]

To assess these emitters in OLEDs, we next measured their photophysical properties as doped films in 2,6-bis(3-(carbazol-9-yl)phenyl)pyridine (26DCzPPy).[19] This material was selected as a host due to the bipolar character, its wide band gap, and its high triplet energy of 2.71 eV. We have employed this host in a study of a somewhat structurally related emitter, **PCP-DiKTa**, to great effect.[15] The spectra of these emitters in 2 wt% doped films in 26DCzPPy are red-shifted by about 10 to 15 nm compared to the respective ones in toluene solution, with the λ_{PL} in the film ranging between 484 and 496 nm (Figure **S84**). Further, a slight broadening of the PL is observed for all emitters. As with the solution-state measurements, the PL of **7-SBF-DiKTa** and **7-SBF-DiKTaSBF** are relatively more narrowband

(FWHM of 32 [166 meV] and 35 nm [173 meV], respectively), whereas the PL of **DiKTaSBF** and **3-SBF-DiKTa** are broader (FWHM of 41 [211 meV] and 49 nm [245 meV], respectively). Upon increasing the doping concentration to 5 and 10 wt%, there is a slight and progressive red-shifting observed in all cases (Figure **S84**).

The Φ_{PL}s of different doping ratios of emitters in 26DCzPPy films were screened, with 2 wt% doping providing the highest values for all emitters. The Φ_{PL} values of the 2 and 5 wt% spin-coated films in 26DCzPPy are compiled in Table **3**. **DiKTaSBF** has the highest Φ_{PL} of 82% in the 2 wt% doped films, which remains at 81% in the 5 wt% doped film. The emitters **7-SBF-DiKTa**, **3-SBF-DiKTa**, and **7-SBF-DiKTaSBF** possess somewhat lower Φ_{PL} values of 71, 72, and 75% as 2 wt% doped films, which contrastingly drop to 59, 58, and 62% upon increasing the doping ratio to 5 wt%. Therefore, 2 wt% proved to be the most promising doping concentration and was therefore selected for further photophysical investigations. Additionally, in all cases a drop in the Φ_{PL} was observed for the aerated films to 58, 54, 40, and 46% for **DiKTaSBF**, **3-SBF-DiKTa**, **7-SBF-DiKTa**, and **7-SBF-DiKTaSBF**, respectively.

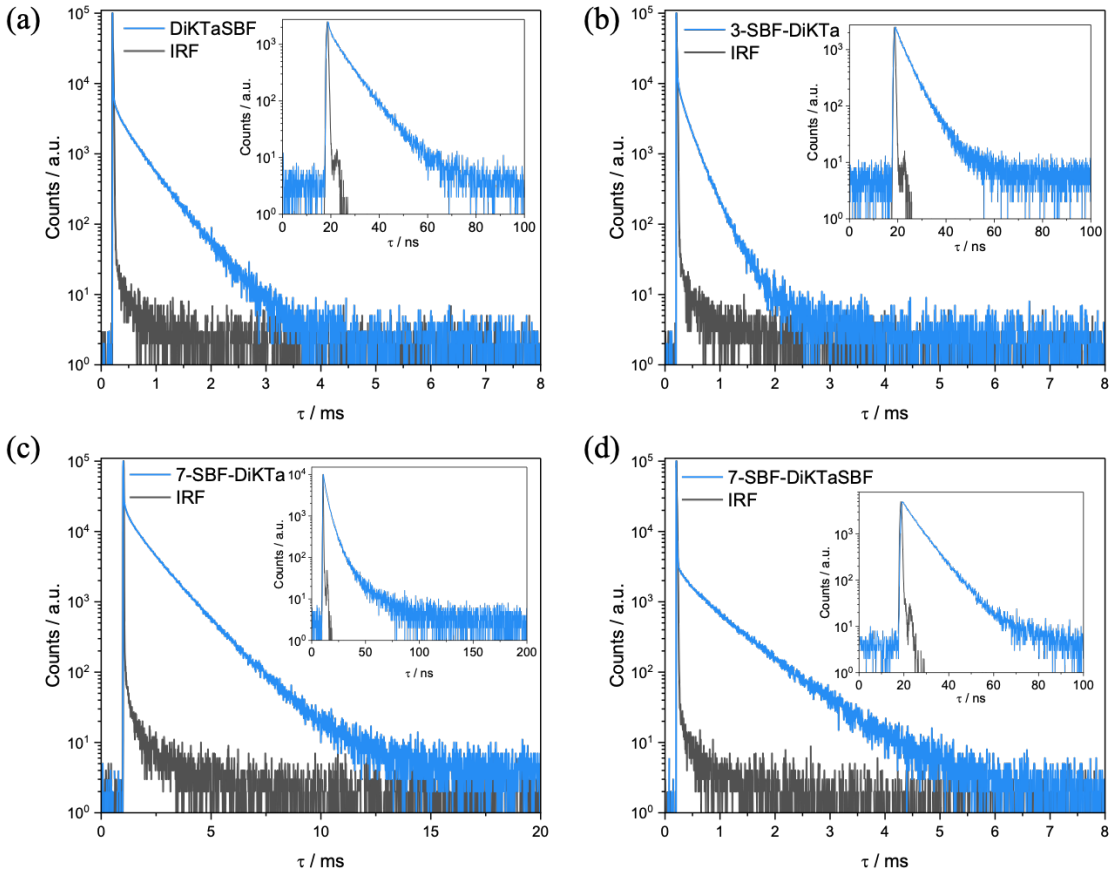

Figure **8**. Time-resolved PL decays of the 2 wt% doped films in 26DCzPPy of (a) **DiKTaSBF**, (b) **3-SBF-DiKTa**, (c) **7-SBF-DiKTa**, and (d) **7-SBF-DiKTaSBFb** with the corresponding instrument response functions (IRF). The prompt fluorescence lifetimes were measured by TCSPC (λ_{exc} = 375 nm), whereas the delayed emission lifetimes were measured by MCS (λ_{exc} = 344 nm).

The PL of the 2 wt% doped films in 26DCzPPy decay with multiexponential kinetics, modelled as biexponential decays for both τ_p and τ_d (Figure **8**). The average prompt lifetimes $\tau_{p,\,avg}$ are similar among the four emitters and in the same range as those determined in toluene, with $\tau_{p,\,avg}$ of between 4.52 and 6.89 ns. The 3-modified derivatives have significantly shorter average delayed lifetimes $\tau_{d,\,avg}$ of 209 and 394 μs for **3-SBF-DiKTa** and **DiKTaSBF**, respectively, compared to the 7-modified derivatives, where the $\tau_{d,\,avg}$ are 632 and 1,163 μs for **7-SBF-DiKTaSBF** and **7-SBF-DiKTa**, respectively.

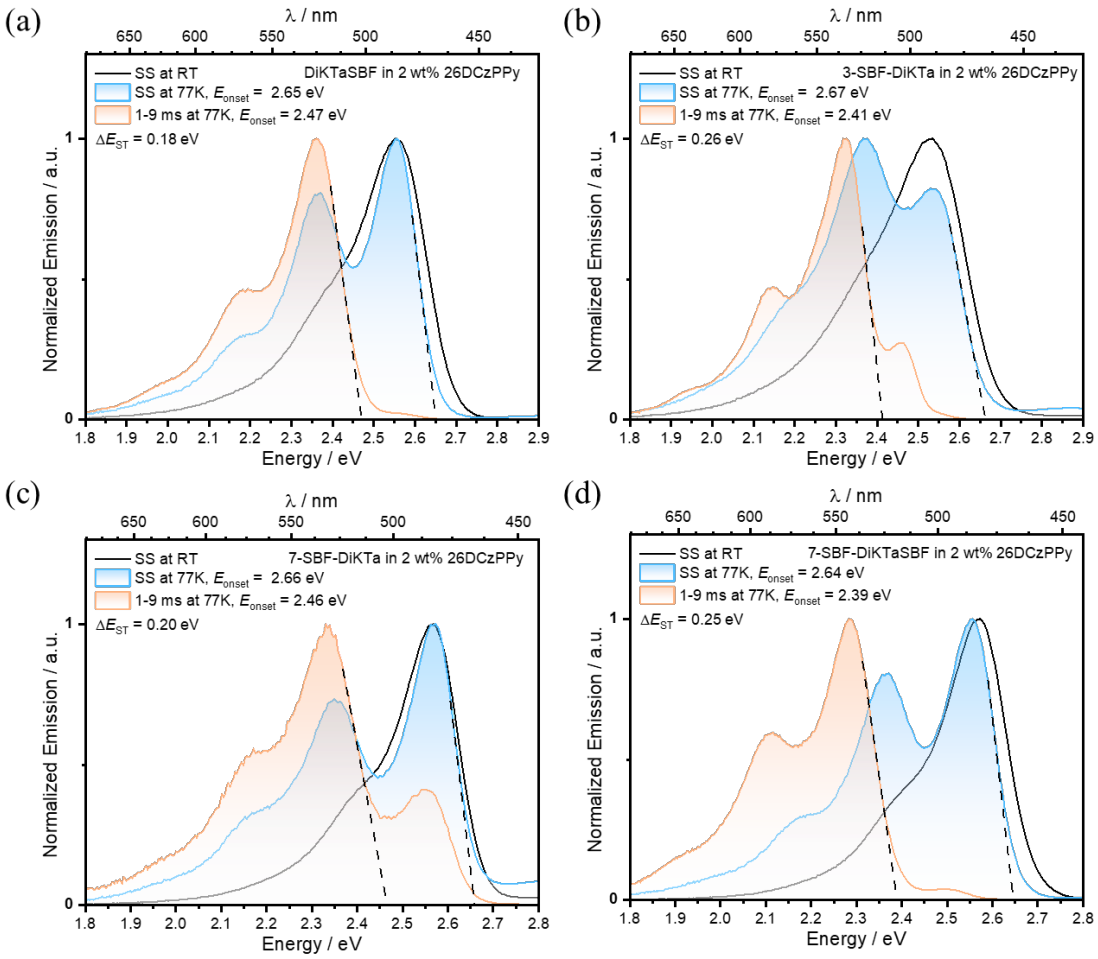

Figure **9**. Steady-state PL and phosphorescence spectra of 2 wt% doped films of (a) **DiKTaSBF**, (b) **3-SBF-DiKTa**, (c) **7-SBF-DiKTa**, and (d) **7-SBF-DiKTaSBF** at 77 K (λ_{exc} = 344 nm) in 26DCzPPy.

The ΔE_{ST} was determined from the onsets of the steady-state PL and phosphorescence spectra in 2 wt% doped films in 26DCzPPy at 77 K (Figure **9**). The ΔE_{ST} values range between 0.18 and 0.26 eV. These values are of similar magnitude to those of **DiKTa** and many of its derivatives, such as 0.20 eV for **DiKTa**,[17] 0.21 eV for **Mes$_3$DiKTa**,[4] and 0.23 eV for **SFQ**,[9] indicating that these four emitters should be TADF. This conclusion was corroborated from the temperature-dependent time-resolved PL measurements (Figure **10**) of the 2 wt% doped films in 26DCzPPy, as the delayed component disappears upon cooling below 200 K, where TADF is arrested.

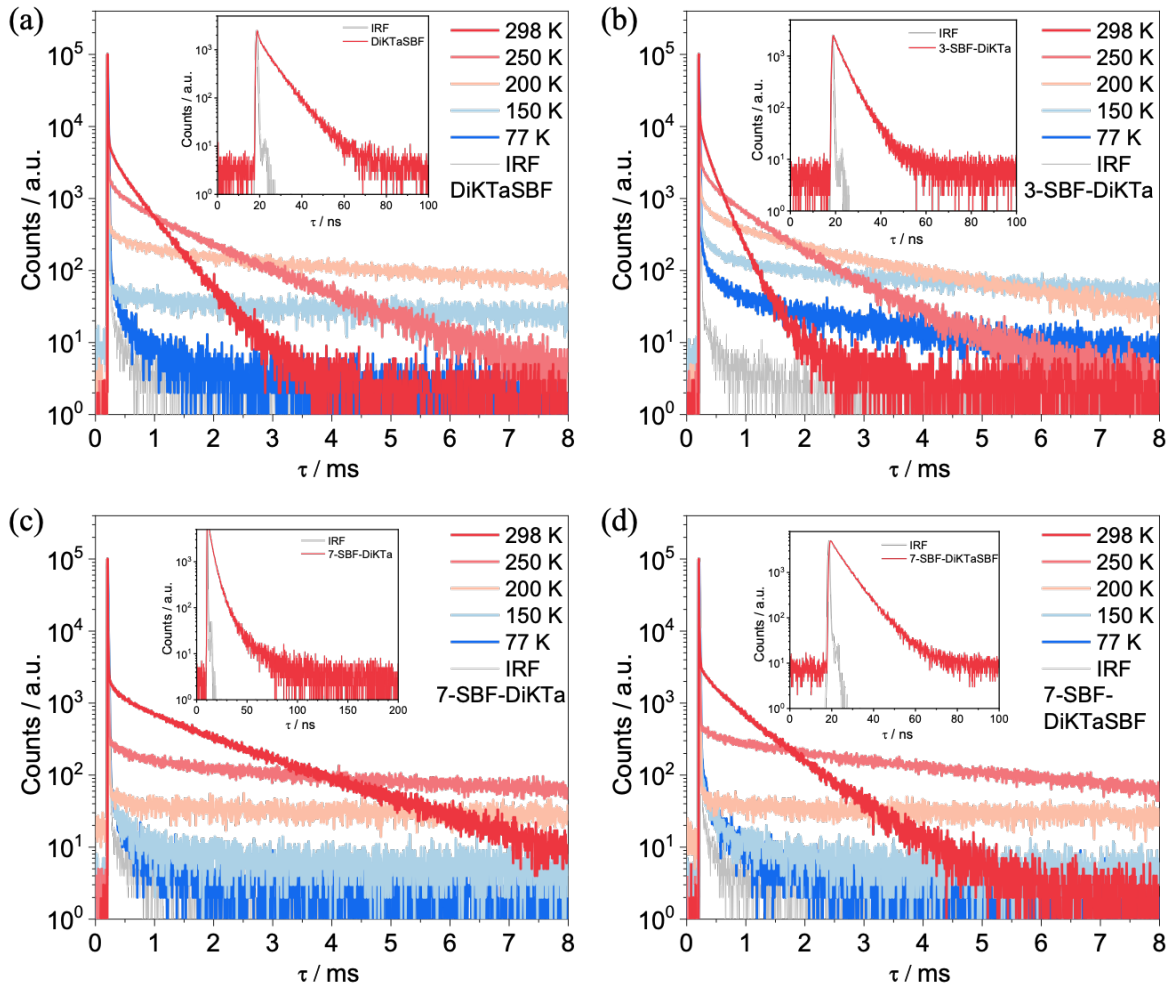

Figure **10**. Temperature-dependent time-resolved PL measurements of the 2 wt% doped films in 26DCzPPy under vacuum (λ_{exc} = 344 nm) of (a) **DiKTaSBF**, (b) **3-SBF-DiKTa**, (c) **7-SBF-DiKTa**, and (d) **7-SBF-DiKTaSBF**. Delayed emission lifetimes were determined by MCS (λ_{exc} = 344 nm). Insets: the prompt PL decays at 300 K measured by TCSPC (λ_{exc} = 375 nm).

Table **3**. Summary of the photophysical properties.

	Solution			**Film**					
	$\lambda_{PL,\ toluene}$ (FWHM) [nm][a]	$\tau_p/\tau_{d,\ toluene}$ [ns/µs][b]	$\Delta E_{ST,\ 2\text{-MeTHF}}$ [eV][c]	$\lambda_{PL,\ 2\ wt\%}$ (FWHM) [nm][d]	$\Phi_{PL,\ 2wt\%}$ in N_2 (air) [%][d]	$\Phi_{PL,\ 5\ wt\%}$ in N_2 (air) [%][d]	τ_p/τ_d [ns/µs][e]	S_1/T_1 [eV][f]	ΔE_{ST} [eV][f]
DiKTa[6]	453 (27)	5.1 / 23	-	466 (40)[g]	70 (mCP)	-	4.5 / 168[g]	2.55 / 2.75[g]	0.20[g]
DiKTaSBF	476 (38)	6.18 / 88.7	0.20	490 (41)	82 (58)	81 (60)	6.96 / 394	2.47 / 2.65	0.18
3-SBF-DiKTa	474 (34)	5.98 / 107	0.22	489 (49)	72 (54)	58 (44)	4.78 / 209	2.41 / 2.67	0.26
7-SBF-DiKTa	470 (26)	5.42 / 71.5	0.25	484 (32)	71 (40)	59 (38)	4.52 / 1163	2.46 / 2.66	0.20
7-SBF-DiKTaSBF	485 (29)	6.00 / 90.5	0.22	496 (35)	75 (46)	62 (43)	6.63 / 632	2.39 / 2.64	0.25

[a] In dilute toluene at 300 K (10^{-5} M, λ_{exc} = 340 nm). [b] In degassed dilute toluene solution (10^{-5} M). τ_p measured by TCSPC λ_{exc} = 375 nm, τ_d measured by MCS, λ_{exc} = 375 nm. [c] Determined from the onsets of the SS PL and phosphorescence spectra in 2-MeTHF at 77 K (λ_{exc} = 340 nm). [d] Spin-coated 2 and 5 wt% thin films in 26DCzPPy (λ_{exc} = 344 nm). [e] In 2 wt% 26DCzPPy film. τ_p measured by TCSPC, λ_{exc} = 375 nm, τ_d measured by MCS, λ_{exc} = 344 nm. [f] Determined from the onsets of the SS-PL and phosphorescence spectra in 2 wt% 26DCzPPy films at 77 K. [g] 2 wt% films in mCP, taken from the literature [6].

The excited-state kinetics were determined following the methodology of Tsuchiya *et al.*,[20] assuming a steady-state approximation and compared to the values for **DiKTa**[21] reported in 2 wt% doped films in mCP using literature photophysical data (Table **4**). The ISC and RISC rate constants of the emitters do not exceed those of **DiKTa** (k_{ISC} of 1.94×10^8 s^{-1} and k_{RISC} of 2.48×10^4 s^{-1}). **7-SBF-DiKTa** has a k_{ISC} of 1.94×10^8 s^{-1}, with k_{ISC} decreasing slightly to 1.78, 1.27, and 1.15×10^8 s^{-1} for **3-SBF-DiKTa**, **7-SBF-DiKTaSBF**, and **DiKTaSBF**, respectively. **DiKTaSBF**, **7-SBF-DiKTa**, and **7-SBF-DiKTaSBF** have k_{RISC} of 9.84, 4.93, and 6.55×10^3 s^{-1}, respectively. The k_{RISC} of **3-SBF-DiKTa** is one order higher in magnitude at 2.15×10^4 s^{-1}. This indicates that the installation of the SBF groups at the 3-position of **DiKTa** leads to derivatives having faster k_{RISC}.

Table **4**. Excited-state rate constants for the films.

	Φ_{PL} /%	k_p /s^{-1} [10^8]	k_d /s^{-1} [10^3]	k_r^S /s^{-1} [10^7]	k_{ISC} /s^{-1} [10^8]	k_{RISC} /s^{-1} [10^3]
DiKTa[a] [21]	46	2.08	4.1	1.42	1.94	24.8
DiKTaSBF[b]	82	1.44	2.54	2.87	1.15	9.84
3-SBF-DiKTa[b]	72	2.09	4.78	3.12	1.78	21.5
7-SBF-DiKTa[b]	75	2.21	0.86	2.75	1.94	4.93
7-SBF-DiKTaSBF[b]	71	1.51	1.58	2.39	1.27	6.55

In [a] 1.5 wt% mCP and [b] 2 wt% 26DCzPPy. Rate constants were calculated using the steady-state approximation[20] (see Supporting Information).

Organic Light-Emitting Diodes

The promising photophysical properties of the emitters encouraged the fabrication of vacuum-deposited OLEDs. The device architecture and the chemical structures of the organic layers are shown in Figure **11a** and **b**, respectively. The OLED structure consisted of: indium tin oxide (ITO)/ 1,4,5,8,9,11-hexaazatriphenylenehexacarbonitrile (HATCN, 5 nm)/ 1,1-bis[(di-4-tolylamino)phenyl]cyclohexane (TAPC, 45 nm)/ 1,3-bis(*N*-carbazolyl)benzene (mCP, 5 nm)/ 26DCzPPy as host (20 nm) with **DiKTaSBF**, **3-SBF-DiKTa**, **7-SBF-DiKTa**, and **7-SBF-DiKTaSBF** as emitter dopants/ 1,3,5-tris(3-pyridyl-3-phenyl)benzene (TmPyPB, 45 nm)/ lithium fluoride (LiF, 1 nm)/ aluminum (Al, 100 nm). Here, HATCN was used as the hole injection layer, TAPC as the hole transport layer, mCP as an exciton blocking layer, TmPyPB as electron transport layer, and LiF to reduce the work function of the top Al electrode. Figure **11c** shows the current density – voltage – luminance (JVL) characteristics of the 2 wt% concentration devices. The turn-on voltage of the OLEDs was between 3.8 – 4.2 V, where devices with **DiKTaSBF** and **3-SBF-DiKTa** showed slightly higher current densities and luminance at the same voltages compared to the devices with the remaining two emitters. The external quantum efficiencies of the devices are shown in Figure **11d** and Table **5**. The devices with **DiKTaSBF** showed an EQE_{max} of 26.1%, an EQE_{100} (at 100 cd m^{-2}) of 16.8%, and an EQE_{1000} (at 1000 cd m^{-2}) of 6.6%. These devices emitted at λ_{EL} of 487 nm, which are close to the λ_{PL} of 490 nm of the thin film of this emitter (Table **3**), with a FWHM of 48 nm (Figure **11e**). The CIE(x, y) coordinates are (0.148, 0.413), as shown in Figure **11f**. The devices with **3-SBF-DiKTa** showed a higher EQE_{max} of 27.0%, which dropped to an EQE_{100} of 20.0% and an EQE_{1000} of 8.8%. The devices emitted at λ_{EL} of 488 nm (FWHM of 52 nm) and have CIE(x, y) coordinates of (0.155, 0.421). The high EQE_{max} of devices with **DiKTaSBF** and **3-SBF-DiKTa** are in accordance with their high Φ_{PL} values of 82 and 72%, respectively. In addition to their high Φ_{PL}, these emitters are preferentially horizontally oriented, with *a* of 72.1 and 70.6% (where 66.6% is isotropic), respectively (Figure **S92**). This contributes to the increased light outcoupling efficiency from these OLEDs.

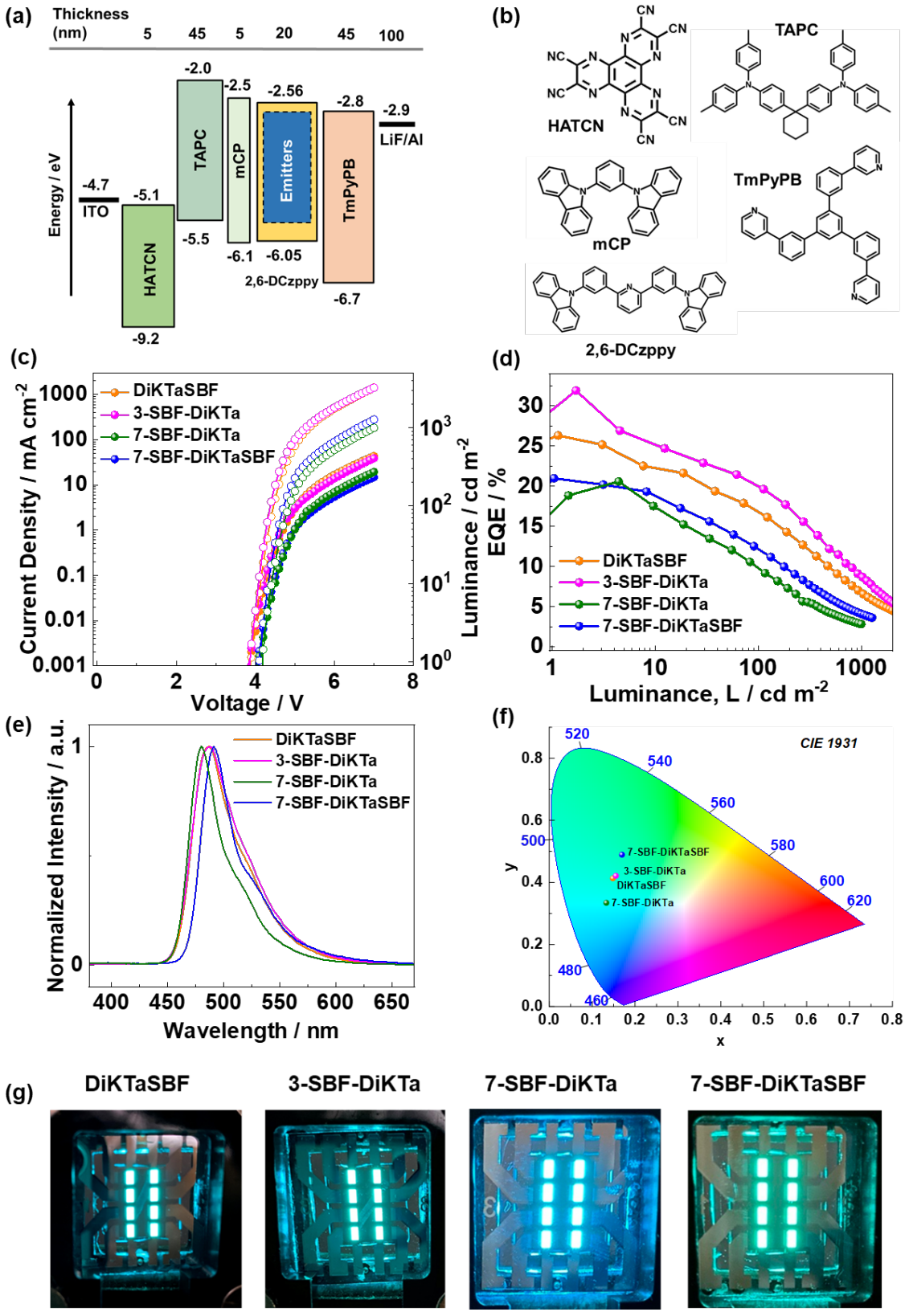

Figure **11**. (a) Schematic of the OLED stack; (b) Chemical structures of the materials used in the devices; (c) Current density-voltage-luminescence (JVL) characteristics with closed circles for J and open circles for L; (d) External quantum efficiency (EQE) vs luminescence; (e) Electroluminescence spectra; (f) CIE coordinates of the devices; (g) Photographs of fabricated OLEDs.

The OLEDs with **7-SBF-DiKTaSBF** showed an EQE_{max} of 20.1%, with an efficiency drop to an EQE_{100} of 12% and an EQE_{1000} of 4%. The λ_{EL} of the devices was at 491 nm (FWHM of 35 nm) and the CIE(x, y) coordinates were (0.169, 0,489). The devices with **7-SBF-DiKTa** also showed similar EQE_{max} of 20.5%, but the efficiency roll-off was more pronounced, with an EQE_{100} of 9.8% and an EQE_{1000} of 2.8%. The emission was slightly blue-shifted as compared to the devices with the other emitters at λ_{EL} of 480 nm (FWHM of 34 nm) and CIE(x, y) coordinates of (0.133, 0.334). The **7-SBF-DiKTa** and **7-SBF-DiKTaSBF** emitters have very similar Φ_{PL} values of 71 and 75%, comparable or slightly lower than the Φ_{PL} of the previous two emitters; however, the EQE_{max} of their OLEDs was notably lower. These emitters showed close to isotropic orientation values of 68.8 and 64.3%, respectively (Figure **S92**). Photographs of the 2 wt% OLEDs are shown in Figure **11g**. OLEDs with higher concentration (5 wt%) of emitters were also fabricated, and these results are shown in Figure **S93**.

We now consider the origin of the efficiency roll-off in these OLEDs. Efficiency roll-off arises from processes involving long-lived triplets and can be mitigated by reducing the triplet population. The triplet population is determined by the interplay of forward and reverse intersystem crossing together (i.e., ISC/RISC) with the radiative rate. To reduce the triplet population and hence reduce efficiency roll-off, the figure of merit (FOM) $\frac{4k_r^S k_{RISC}}{3k_r^S+4k_{ISC}}$ should be maximized.[22] We show this FOM in Table **5** and find it is highest for the device with **3-SBF-DiKTa**, slightly lower for the device with **DiKTaSBF**, substantially lower for the device with **7-SBF-DiKTaSBF** and even lower for the device with **7-SBF-DiKTa**. Accordingly, we would expect efficiency roll-off to be smallest for the device with **3-SBF-DiKTa** and highest for the device with **7-SBF-DiKTa**. We take EQE_{1000}/EQE_{max} as a measure of the efficiency roll-off (Table **5**), where lower values of EQE_{1000}/EQE_{max} indicate more severe efficiency roll-off. We find that the trend in device efficiency roll-off is correlated with the trend in FOM.

Table **5**. Device performance for OLEDs with 2 wt% of emitter.

Emitter	**EQE_{max} /EQE_{100} /EQE_{1000} [%]**	**λ_{PL} [nm]**	**λ_{EL} [nm]**	**FWHM [nm]**	**CIE (x, y)**	**$\frac{EQE_{1000}}{EQE_{max}}$ [%]**	**FOM[22] ($\frac{4k_r^S k_{RISC}}{3k_r^S+4k_{ISC}}$)**
DiKTaSBF	26.1 /16.8 / 6.6	490	487	48	0.148, 0.413	25.3	1700
3-SBF-DiKTa	27.0 /20.0 /8.8	489	488	52	0.155, 0.421	32.6	2170
7-SBF-DiKTa	20.5 /9.8 /2.8	484	480	34	0.133, 0.334	13.7	555
7-SBF-DiKTaSBF	20.1 /12.0 /4.0	496	491	35	0.169, 0.489	19.9	827

Conclusion

We have designed four novel narrowband sky-blue **DiKTa**-based SBF-modified MR-TADF emitters **DiKTaSBF**, **3-SBF-DiKTa**, **7-SBF-DiKTa** and **7-SBF-DiKTaSBF**, differing in number, position, and incorporation type of the SBF unit. Structure-property relationships were identified, and there is a significant impact of the substituent position on the photophysical properties and corresponding device performance. Substitution at the 3-position led to devices with higher efficiencies, with EQE_{max} of up to 27.0% and alleviated efficiency roll-off. In contrast, substitution at the 7-position favored narrowband emission, with FWHM of 34 nm. Further, no significant impact on the optoelectronic properties was observed between fusion and coupling of the SBF unit. The combination of fusion at the 3-position and substitution at the 7-position resulted in nearly identical optoelectronic behavior as the emitter having an SBF substituent solely at the 7-position. These results show the significant impact of the modification site on the photophysical and optoelectronic behavior, highlighting the importance of these considerations for the design of future compounds.

Acknowledgements

J.H. thanks the Studienstiftung des deutschen Volkes. S.W. thanks the China Scholarship Council (201906250199). The authors thank Dr. Tomas Matulaitis for help with some of the photophysical characterization. The authors acknowledge the support of Luca Schichtel for his help with the synthesis. The authors acknowledge the help of Dr. Andreas Rapp for the low-temperature ^{1}H NMR measurements. The authors thank Dr. Gavin Peters for conducting the TGA and DSC measurements. The authors acknowledge the support from the state of Baden-Württemberg through bwHPC. This project has been partly funded by the European Union Horizon 2021 research and innovation programme under grant agreement No. 101073045 (TADFsolutions) and the EPSRC grant EP/X026175/1. We thank the EPSRC (EP/Z535291/1, EP/W007517/1, and EP/W015137/1) for financial support.

Author Contributions

CRediT: J.H.: conceptualization, data curation, formal analysis, investigation, methodology, visualization, writing - original draft, writing - review & editing. S.W.: conceptualization, data curation, formal analysis, investigation, methodology, writing – review & editing. H.H.: data curation, formal analysis, investigation, methodology, visualization, writing - original draft, writing - review & editing. M.S.: investigation. M.F.: investigation, writing – review & editing. Y.T.W.: data curation, investigation, methodology, writing – review & editing. M.N.: formal analysis, investigation, writing – review & editing. O.F.: formal analysis, investigation, writing – review & editing. B.L.: investigation, methodology, supervision. I.D.W.S.: conceptualization, funding acquisition, methodology, project administration, resources, supervision, writing – review & editing. S.B.: conceptualization, funding acquisition, methodology, project administration, resources, supervision, writing – review & editing.

E.Z.-C.: conceptualization, funding acquisition, methodology, project administration, resources, supervision, writing – review & editing.

Supporting Information

Synthetic procedures, ^{1}H NMR and ^{13}C NMR spectra, HRMS and reverse phase and gel permeation (GPC) HPLC; supplementary computational data and coordinates; Crystallographic data, CCDC 2442317 (**DiKTaSBF**) and 2440880 (**7-SBF-DiKTaSBF**). Supplementary photophysical and OLED data.

Data Availability Statement

The research data supporting this publication can be accessed at https://dx.doi.org/10.14272/collection/JAH_2023-06-01.

References

[1] T. Hatakeyama, K. Shiren, K. Nakajima, S. Nomura, S. Nakatsuka, K. Kinoshita, J. Ni, Y. Ono, T. Ikuta, *Adv. Mater.* **2016**, *28*, 2777.

[2] a) S. Madayanad Suresh, D. Hall, D. Beljonne, Y. Olivier, E. Zysman-Colman, *Adv. Funct. Mater.* **2020**, *30*, 1908677; b) J. M. Dos Santos, D. Hall, B. Basumatary, M. Bryden, D. Chen, P. Choudhary, T. Comerford, E. Crovini, A. Danos, J. De, S. Diesing, M. Fatahi, M. Griffin, A. K. Gupta, H. Hafeez, L. Hämmerling, E. Hanover, J. Haug, T. Heil, D. Karthik, S. Kumar, O. Lee, H. Li, F. Lucas, C. F. R. Mackenzie, A. Mariko, T. Matulaitis, F. Millward, Y. Olivier, Q. Qi, I. D. W. Samuel, N. Sharma, C. Si, L. Spierling, P. Sudhakar, D. Sun, E. Tankelevičiūtė, M. Duarte Tonet, J. Wang, T. Wang, S. Wu, Y. Xu, L. Zhang, E. Zysman-Colman, *Chem. Rev.* **2024**, *124*, 13736. c) G. Hong, X. Gan, C. Leonhardt, Z. Zhang, J.Seibert, J.M. Busch, S. Bräse, *Adv. Mater*. **2021**, *33*, 2005630.

[3] Y. Yuan, X. Tang, X.-Y. Du, Y. Hu, Y.-J. Yu, Z.-Q. Jiang, L.-S. Liao, S.-T. Lee, *Adv. Opt. Mater.* **2019**, *7*, 1801536.

[4] D. Hall, S. M. Suresh, P. L. dos Santos, E. Duda, S. Bagnich, A. Pershin, P. Rajamalli, D. B. Cordes, A. M. Z. Slawin, D. Beljonne, A. Köhler, I. D. W. Samuel, Y. Olivier, E. Zysman-Colman, *Adv. Opt. Mater.* **2020**, *8*, 1901627.

[5] X. Li, Y.-Z. Shi, K. Wang, M. Zhang, C.-J. Zheng, D.-M. Sun, G.-L. Dai, X.-C. Fan, D.-Q. Wang, W. Liu, Y.-Q. Li, J. Yu, X.-M. Ou, C. Adachi, X.-H. Zhang, *ACS Appl. Mater. Interfaces* **2019**, *11*, 13472.

[6] S. Wu, A. Kumar Gupta, K. Yoshida, J. Gong, D. Hall, D. B. Cordes, A. M. Z. Slawin, I. D. W. Samuel, E. Zysman-Colman, *Angew. Chem. Int. Ed.* **2022**, *61*, e202213697.

[7] F. Tenopala-Carmona, O. S. Lee, E. Crovini, A. M. Neferu, C. Murawski, Y. Olivier, E. Zysman-Colman, M. C. Gather, *Adv. Mater.* **2021**, *33*, 2100677.

[8] Y.-K. Qu, D.-Y. Zhou, F.-C. Kong, Q. Zheng, X. Tang, Y.-H. Zhu, C.-C. Huang, Z.-Q. Feng, J. Fan, C. Adachi, L.-S. Liao, Z.-Q. Jiang, *Angew. Chem. Int. Ed.* **2022**, *61*, e202201886.

[9] Y.-J. Yu, Z.-Q. Feng, X.-Y. Meng, L. Chen, F.-M. Liu, S.-Y. Yang, D.-Y. Zhou, L.-S. Liao, Z.-Q. Jiang, *Angew. Chem. Int. Ed.* **2023**, *62*, e202310047.

[10] H.-Y. Yan, D.-Y. Zhou, S.-J. Ge, Y.-J. Yu, H.-T. Yuan, R.-H. Liu, Y.-J. Yang, Y. Wang, L.-S. Liao, Z.-Q. Jiang, *Small* **2025**, *21*, 2502915.

[11] L. Wu, C. Liu, D. Liu, D. Li, W. Li, J. Zhang, X. Mu, Z. Xin, B. Liu, H. Qi, Z. Wang, D. Liu, S.-J. Su, Y. Zhou, S. Wu, Z. Ge, *Angew. Chem. Int. Ed.* **2025**, *64*, e202504723.

[12] X. Qiu, G. Tian, C. Lin, Y. Pan, X. Ye, B. Wang, D. Ma, D. Hu, Y. Luo, Y. Ma, *Adv. Opt. Mater.* **2021**, *9*, 2001845.

[13] D. Sun, S. M. Suresh, D. Hall, M. Zhang, C. Si, D. B. Cordes, A. M. Z. Slawin, Y. Olivier, X. Zhang, E. Zysman-Colman, *Mater. Chem. Front.* **2020**, *4*, 2018.

[14] D. Hall, J. C. Sancho-García, A. Pershin, G. Ricci, D. Beljonne, E. Zysman-Colman, Y. Olivier, *J. Chem. Theory Comput.* **2022**, *18*, 4903.
[15] Y. Xu, H. Hafeez, J. Seibert, S. Wu, J. S. O. Ortiz, J. Crassous, S. Bräse, I. D. Samuel, E. Zysman-Colman, *Adv. Funct. Mater.* **2024**, 2402036.
[16] N. G. Connelly, W. E. Geiger, *Chem. Rev.* **1996**, *96*, 877.
[17] S. Wu, Y.-N. Hu, J. Wang, D. Sun, K. Wang, X.-H. Zhang, E. Zysman-Colman, *J. Mater. Chem. C* **2024**, *12*, 6177.
[18] C. M. Cardona, W. Li, A. E. Kaifer, D. Stockdale, G. C. Bazan, *Adv. Mater.* **2011**, *23*, 2367.
[19] S.-J. Su, C. Cai, J. Kido, *Chem. Mat.* **2011**, *23*, 274.
[20] Y. Tsuchiya, S. Diesing, F. Bencheikh, Y. Wada, P. L. dos Santos, H. Kaji, E. Zysman-Colman, I. D. W. Samuel, C. Adachi, *J. Phys. Chem. A* **2021**, *125*, 8074.
[21] S. Wu, L. Zhang, J. Wang, A. Kumar Gupta, I. D. W. Samuel, E. Zysman-Colman, *Angew. Chem. Int. Ed.* **2023**, *62*, e202305182.
[22] S. Diesing, L. Zhang, E. Zysman-Colman, I. D. W. Samuel, *Nature* **2024**, *627*, 747.

Table of Contents

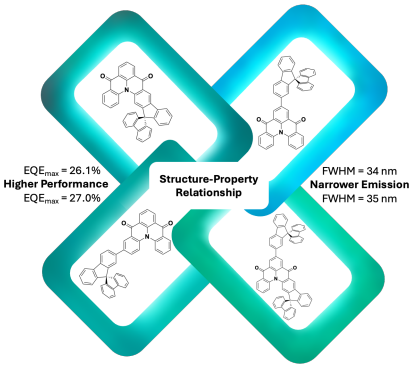

The impact of decorating the multiresonant thermally activated delayed fluorescence (MR-TADF) emitter DiKTa with 9,9'-spirobifluorene units was explored with regard to number, position, and incorporation type. Four novel sky-blue narrowband MR-TADF emitters have been developed and in the OLED devices a structure-property relationship was observed with modification in 3-position favoring performance while modification in 7-position favored color purity.